Published for SISSA by Springer

Received: April 3, 2012
Accepted: June 6, 2012
Published: June 25, 2012

Higgs boson production at the LHC: transverse momentum resummation effects in the $H \to \gamma\gamma$, $H \to WW \to l\nu l\nu$ and $H \to ZZ \to 4l$ decay modes

Daniel de Florian,[a,b] **Giancarlo Ferrera,**[b,c] **Massimiliano Grazzini**[b,1] **and Damiano Tommasini**[b,d]

[a] *Departamento de Física, FCEYN, Universidad de Buenos Aires, 1428 Pabellón 1 Ciudad Universitaria, Capital Federal, Argentina*

[b] *Institut für Theoretische Physik, Universität Zürich, CH-8057 Zürich, Switzerland*

[c] *Dipartimento di Fisica, Università di Milano and INFN — Sezione di Milano, I-20133 Milan, Italy*

[d] *Dipartimento di Fisica e Astronomia, Università di Firenze and INFN — Sezione di Firenze, I-50019 Sesto Fiorentino, Florence, Italy*

E-mail: deflo@df.uba.ar, giancarlo.ferrera@mi.infn.it, grazzini@physik.uzh.ch, tommasini@fi.infn.it

Abstract: We consider Standard Model Higgs boson production through gluon-gluon fusion in hadron collisions. We combine the calculation of the next-to-next-to-leading order QCD corrections to the inclusive cross section with the resummation of multiple soft-gluon emissions at small transverse momenta up to next-to-next-to-leading logarithmic accuracy. The calculation is implemented in the numerical program HRes and allows us to retain the full kinematics of the Higgs boson and of its decay products. We present selected numerical results for the signal cross section at the LHC ($\sqrt{s} = 8\,\text{TeV}$), in the $H \to \gamma\gamma$, $H \to WW \to l\nu l\nu$ and $H \to ZZ \to 4l$ decay channels by using the nominal cuts applied in current Higgs boson searches by the ATLAS and CMS collaborations.

Keywords: Higgs Physics, Resummation

ArXiv ePrint: 1203.6321

[1] On leave of absence from INFN, Sezione di Firenze, Sesto Fiorentino, Florence, Italy.

doi:10.1007/JHEP06(2012)132

JHEP06(2012)132

Contents

1 Introduction

One of the main tasks of the LHC program is the search for the Higgs boson [1–3] and the study of its properties (mass, couplings, decay widths).

The LHC, after a successful start of pp collisions in 2009 and 2010, has been operated at a centre-of-mass energy of 7 TeV in 2011, and data corresponding to an integrated luminosity of 5.7 fb^{-1} have been accumulated. These data already allowed the ATLAS [4] and CMS [5] experiments to shrink the allowed mass range for the Standard Model (SM) Higgs boson H considerably by essentially excluding the Higgs bosons in the mass range $\mathcal{O}(130\,\text{GeV}) < m_H < \mathcal{O}(600\,\text{GeV})$, while observing an excess of Higgs boson candidate events around $m_H = 125\,\text{GeV}$. An update of the Tevatron results [6] with up to 10 fb^{-1} integrated luminosity shows a broad excess of events in the region $115 - 135\,\text{GeV}$. More data from the LHC 2012 run, that will be operated at a centre-of-mass energy of 8 TeV, are needed to say whether these excesses really correspond to a Higgs signal or are just statistical fluctuations.

In this paper we consider the production of the SM Higgs boson by the gluon fusion mechanism and its decays $H \to \gamma\gamma$, $H \to WW$ and $H \to ZZ$. The gluon fusion process $gg \to H$ [7], through a heavy-quark loop, is the main production mechanism of the SM Higgs boson at hadron colliders. The corresponding cross section is typically at least one order of magnitude larger than the cross section in the other production channels (vector boson fusion, associated production...), and becomes comparable with the cross section for vector boson fusion only at high Higgs boson masses. It is thus essential to achieve reliable theoretical predictions for the gluon fusion cross section and the associated distributions. The dynamics of the gluon fusion mechanism is driven by strong interactions.

JHEP06(2012)132

Thus, accurate studies of the effect of QCD radiative corrections are mandatory to obtain precise theoretical predictions.

The leading order (LO) cross section is proportional to α_S^2, α_S being the QCD coupling. The QCD radiative corrections to the total cross section have been computed at the next-to-leading order (NLO) in refs. [8–10] and found to be of the same order as the LO contribution. The next-to-next-to-leading order (NNLO) corrections have been computed in refs. [11–13] and their effect is moderate: for a light Higgs, they increases the NLO cross result by about 25% at the LHC ($\sqrt{s} = 8\,\text{TeV}$). We recall that all the NNLO results have been obtained by using the large-M_t approximation, M_t being the mass of the top quark. Corrections beyond this approximation have been considered in refs. [14–19].

The NNLO result mentioned above is certainly important, but it refers to a fully inclusive cross section. The impact of higher-order corrections generally depends on the selection cuts used in the experimental analysis and also the shape of the distributions is typically affected by the applied cuts.

A first step in the direction of taking selection cuts into account was taken in ref. [20], where the inclusive cross section with a jet veto was computed at NNLO. The first NNLO calculation of the Higgs production cross section that fully takes into account experimental cuts was reported in ref. [21, 22], in the case of the decay mode $H \to \gamma\gamma$. In ref. [23] the calculation was extended to the decay mode $H \to WW \to l\nu l\nu$. An independent NNLO calculation of the Higgs production cross section has been presented in refs. [24, 25], and implemented in the parton-level Monte Carlo program `HNNLO`. Such program allows the user to evaluate the Higgs production cross section with arbitrary kinematical cuts and includes the decay $H \to \gamma\gamma$, $H \to WW \to l\nu l\nu$ and $H \to ZZ \to 4$ leptons.

Unfortunately, fixed order calculations may suffer from perturbative instabilities when different energy scales are involved. An example is the transverse momentum p_T spectrum of the Higgs boson. In the small-p_T region ($p_T \ll m_H$), the convergence of the fixed-order expansion is spoiled by the presence of large logarithmic terms, $\alpha_S^n \ln^m(m_H^2/p_T^2)$. To obtain reliable predictions, these logarithmically-enhanced terms have to be systematically resummed to all perturbative orders [26, 27]–[39]. It is then important to consistently match the resummed and fixed-order calculations at intermediate values of p_T, in order to obtain accurate QCD predictions for the entire range of transverse momenta. In the case of Higgs boson production the resummation has been performed up to next-to-next-to-leading logarithmic (NNLL) accuracy [38, 40] and matched to the fixed order $\mathcal{O}(\alpha_S^4)$ result valid at large transverse momenta [42–44]. The calculation has been implemented in a numerical program, named `HqT` [45] that has been used by the experimental collaborations at the Tevatron and the LHC for a few years. In ref. [46] the calculation has been extended to include the rapidity dependence of the Higgs boson. In ref. [47] we have improved the calculation of ref. [38] by implementing the exact form of the NNLO coefficients of ref. [48][1] and the value for the coefficient $A^{(3)}$ derived in ref. [49]. The corresponding computation is implemented in a new version of `HqT`.

[1]The results of ref. [38, 46] were based on a reasonable approximation of these NNLO hard-collinear coefficients.

JHEP06(2012)132

In this paper we take one step forward with respect to the work of refs. [38, 46, 47]. We start from the doubly differential cross section, including transverse-momentum resummation and rapidity dependence [46] and we implement the hard collinear coefficients of ref. [48] that, together with the exact form of the coefficient $A^{(3)}$ [49], allow us to control the resummation at full NNLL accuracy. We then include the Higgs boson decay and implement the ensuing result into an efficient Higgs event generator, that is able to simulate the full kinematics of the Higgs boson and of its decay products. The resummed result is finally matched with the fixed order NNLO computation of ref. [24, 25] to obtain a prediction that is everywhere as good as the NNLO result, but includes the resummation of the logarithmically enhanced contributions at small transverse momenta. The exact form of the second order hard-collinear coefficients of ref. [48] permits a fully consistent matching with the NNLO rapidity distribution upon integration over p_T. The calculation is implemented in a new numerical program called `HRes`, that embodies the features of `HNNLO` and `HqT`. We present a selection of numerical results that can be obtained with our program for Higgs boson production at the LHC ($\sqrt{s} = 8\,\text{TeV}$) up to NNLL+NNLO accuracy. We consider the decay modes $H \to \gamma\gamma$, $H \to WW \to l\nu l\nu$ and $H \to ZZ \to 4l$ and we compare the resummed results with the corresponding fixed order results, up to the NNLO accuracy, obtained with the `HNNLO` numerical code.

The paper is organized as follows. In section 2 we recall the main features of our resummation formalism and we introduce our NNLL+NNLO numerical program `HRes`. In section 3 we present our numerical predictions at the LHC. In section 4 we summarize our results.

2 Transverse momentum resummation and the HRes program

We start this section by briefly recalling the resummation formalism of refs. [37, 38, 46]. We consider the inclusive hard-scattering process

$$h_1(p_1) + h_2(p_2) \to H(y, p_T, m_H) + X \ , \tag{2.1}$$

where the collision of the two hadrons h_1 and h_2 with momenta p_1 and p_2 produces the Higgs boson H with transverse momentum p_T and rapidity y (defined in the centre-of-mass frame) accompanied by an arbitrary and undetected final state X. The centre-of-mass energy of the colliding hadrons is denoted by $\sqrt{s}$.

According to the QCD factorization theorem, the doubly differential cross section for this process reads

$$\begin{aligned}\frac{d\sigma}{dy\,dp_T^2}(y, p_T, m_H, s) = \sum_{a_1,a_2} \int_0^1 dx_1 \int_0^1 dx_2\, f_{a_1/h_1}(x_1, \mu_F^2)\, f_{a_2/h_2}(x_2, \mu_F^2) \\ \times \frac{d\hat{\sigma}_{a_1 a_2}}{d\hat{y}\,dp_T^2}(\hat{y}, p_T, m_H, \hat{s}; \alpha_S(\mu_R^2), \mu_R^2, \mu_F^2) \ ,\end{aligned} \tag{2.2}$$

where $f_{a/h}(x, \mu_F^2)$ ($a = q_f, \bar{q}_f, g$) are the parton densities of the colliding hadrons at the factorization scale μ_F, $d\hat{\sigma}_{ab}$ are the partonic cross sections, and μ_R is the renormalization

JHEP06(2012)132

scale. The rapidity, $\hat{y}$, and the centre-of-mass energy, $\hat{s}$, of the partonic cross section (subprocess) are related to the corresponding hadronic variables y and s as:

$$\hat{y} = y - \frac{1}{2} \ln \frac{x_1}{x_2} \,, \qquad \hat{s} = x_1 x_2 s \ . \tag{2.3}$$

The partonic cross section $d\hat{\sigma}_{ab}$ is computable in QCD perturbation theory but its series expansion in $\alpha_{\rm S}$ contains the logarithmically-enhanced terms, $(\alpha_{\rm S}^n/p_T^2)\,\ln^m(m_H^2/p_T^2)$, that we want to resum.

To this purpose, the partonic cross section is rewritten as the sum of two terms,

$$\frac{d\hat{\sigma}_{a_1a_2}}{d\hat{y}\,dp_T^2} = \frac{d\hat{\sigma}^{(\rm res.)}_{a_1a_2}}{d\hat{y}\,dp_T^2} + \frac{d\hat{\sigma}^{(\rm fin.)}_{a_1a_2}}{d\hat{y}\,dp_T^2} \ . \tag{2.4}$$

The logarithmically-enhanced contributions are embodied in the 'resummed' component $d\hat{\sigma}^{(\rm res.)}_{a_1a_2}$. The 'finite' component $d\hat{\sigma}^{(\rm fin.)}_{a_1a_2}$ is free of such contributions, and it can be computed by a truncation of the perturbative series at a given fixed order. In particular we compute $d\hat{\sigma}^{(\rm fin.)}_{a_1a_2}$ starting from $[d\hat{\sigma}_{a_1a_2}]_{\rm f.o.}$, the usual perturbative series truncated at a given fixed order in $\alpha_{\rm S}$, and we subtract the perturbative truncation of the resummed component at the same order:

$$\left[\frac{d\hat{\sigma}^{(\rm fin.)}_{a_1a_2}}{d\hat{y}\,dp_T^2}\right]_{\rm f.o.} = \left[\frac{d\hat{\sigma}_{a_1a_2}}{d\hat{y}\,dp_T^2}\right]_{\rm f.o.} - \left[\frac{d\hat{\sigma}^{(\rm res.)}_{a_1a_2}}{d\hat{y}\,dp_T^2}\right]_{\rm f.o.} \ . \tag{2.5}$$

The resummation procedure of the logarithmic terms has to be carried out [28]–[33–35] in the impact-parameter space, to correctly take into account the kinematics constraint of transverse-momentum conservation. The resummed component of the partonic cross section is then obtained by performing the inverse Fourier (Bessel) transformation with respect to the impact parameter b. We write[2]

$$\frac{d\hat{\sigma}^{(\rm res.)}_{a_1a_2}}{d\hat{y}\,dp_T^2}(\hat{y}, p_T, m_H, \hat{s}; \alpha_{\rm S}) = \frac{m_H^2}{\hat{s}} \int_0^\infty db\, \frac{b}{2}\, J_0(bp_T)\, \mathcal{W}_{a_1a_2}(\hat{y}, b, m_H, \hat{s}; \alpha_{\rm S}) \,, \tag{2.6}$$

where $J_0(x)$ is the 0th-order Bessel function, and the factor $\mathcal{W}$ embodies the all-order dependence on the large logarithms $\ln(m_H^2 b^2)$ at large b, which correspond to $\ln(m_H^2/p_T^2)$ terms in p_T space.

In the case of the p_T cross section integrated over the rapidity, the resummation of the large logarithms is better expressed [37, 38] by defining the N-moments $\mathcal{W}_N$ of $\mathcal{W}$ with respect to $z = m_H^2/\hat{s}$ at fixed m_H. In the present case, in which we want to keep the dependence on the rapidity into account, we consider 'double' (N_1, N_2)-moments with respect to the two variables $z_1 = e^{+\hat{y}} m_H/\sqrt{\hat{s}}$ and $z_2 = e^{-\hat{y}} m_H/\sqrt{\hat{s}}$ at fixed m_H (note that $0 < z_i < 1$). We thus introduce $\mathcal{W}^{(N_1,N_2)}$ as follows [46]:

$$\mathcal{W}^{(N_1,N_2)}_{a_1a_2}(b, m_H; \alpha_{\rm S}) = \int_0^1 dz_1\, z_1^{N_1-1} \int_0^1 dz_2\, z_2^{N_2-1}\ \mathcal{W}_{a_1a_2}(\hat{y}, b, m_H, \hat{s}; \alpha_{\rm S}) \,. \tag{2.7}$$

[2] In the following equations, the functional dependence on the scales μ_R and μ_F is understood.

JHEP06(2012)132

More generally, for any function $h(y;z)$ with $|y| < -\ln\sqrt{z}$ and $0 < z < 1$ we can define (N_1, N_2) Mellin moments as

$$h^{(N_1,N_2)} \equiv \int_0^1 dz_1\, z_1^{N_1-1} \int_0^1 dz_2\, z_2^{N_2-1}\, h(y;z)\;, \quad \text{where}: y = \frac{1}{2}\ln\frac{z_1}{z_2}\;,\; z = z_1 z_2\;. \tag{2.8}$$

The convolution structure of the QCD factorization formula (2.2) is easily diagonalized by considering (N_1, N_2)-moments:

$$d\sigma^{(N_1,N_2)} = \sum_{a_1,a_2} f_{a_1/h_1,N_1+1}\, f_{a_2/h_2,N_2+1}\, d\hat{\sigma}_{a_1a_2}^{(N_1,N_2)}\;, \tag{2.9}$$

where $f_{a/h,N} = \int_0^1 dx\, x^{N-1} f_{a/h}(x)$ are the customary N-moments of the parton distributions.

The use of Mellin moments also simplifies the resummation structure of the logarithmic terms in $d\hat{\sigma}_{a_1a_2}^{(\text{res.})\,(N_1,N_2)}$. The perturbative factor $\mathcal{W}_{a_1a_2}^{(N_1,N_2)}$ can indeed be organized in exponential form as follows:

$$\mathcal{W}^{(N_1,N_2)}(b, m_H; \alpha_S) = \mathcal{H}^{(N_1,N_2)}(m_H, \alpha_S; m_H^2/Q^2)\, \exp\{\mathcal{G}^{(N_1,N_2)}(\alpha_S, \widetilde{L}; m_H^2/Q^2)\}\;, \tag{2.10}$$

where

$$\widetilde{L} = \ln\left(\frac{Q^2\, b^2}{b_0^2} + 1\right)\;, \tag{2.11}$$

$b_0 = 2e^{-\gamma_E}$ ($\gamma_E = 0.5772\ldots$ is the Euler number) and, to simplify the notation, the dependence on the flavour indeces has been understood. The scale $Q \sim m_H$ in eq. (2.11), named resummation scale, parametrizes the arbitrariness in the resummation procedure. Its role is analogous to the role played by the renormalization (factorization) scale in the context of the renormalization (factorization) procedure. Although the resummed cross section does not depend on Q when evaluated at all perturbative orders, its explicit dependence on Q appears after truncation of the resummed expression at a given logarithmic accuracy.

The function $\mathcal{H}^{(N_1,N_2)}$ does not depend on the impact parameter b and, therefore, its evaluation does not require resummation of large logarithmic terms. It can be expanded in powers of α_S as

$$\mathcal{H}^{(N_1,N_2)} = \sigma_0(\alpha_S, m_H)\left[1 + \frac{\alpha_S}{\pi}\,\mathcal{H}^{(N_1,N_2)\,(1)} + \left(\frac{\alpha_S}{\pi}\right)^2 \mathcal{H}^{(N_1,N_2)\,(2)} + \ldots\right]\;, \tag{2.12}$$

where $\sigma_0(\alpha_S, m_H)$ is the lowest-order partonic cross section for Higgs boson production. The form factor $\exp\{\mathcal{G}\}$ includes the complete dependence on b and, in particular, it contains all the terms that order-by-order in α_S are logarithmically divergent when $b \to \infty$. The functional dependence on b is expressed through the large logarithmic terms $\alpha_S^n \widetilde{L}^m$ with $1 \le m \le 2n$. More importantly, all the logarithmic contributions to $\mathcal{G}$ with $n+2 \le m \le 2n$ are vanishing. Thus, the exponent $\mathcal{G}$ can systematically be expanded in powers of α_S, at fixed value of $\lambda = \alpha_S \widetilde{L}$, as follows:

$$\begin{aligned}\mathcal{G}^{(N_1,N_2)}(\alpha_S, \widetilde{L}; m_H^2/Q^2) = {} & \widetilde{L}\, g^{(1)}(\alpha_S\widetilde{L}) + g^{(2)\,(N_1,N_2)}(\alpha_S\widetilde{L}; m_H^2/Q^2) \\ & + \frac{\alpha_S}{\pi}\, g^{(3)\,(N_1,N_2)}(\alpha_S\widetilde{L}; m_H^2/Q^2) + \ldots\;.\end{aligned} \tag{2.13}$$

JHEP06(2012)132

The term $\widetilde{L}g^{(1)}$ collects the leading logarithmic (LL) contributions $\alpha_{\rm S}^n\widetilde{L}^{n+1}$; the function $g^{(2)}$ includes the next-to-leading logarithmic (NLL) contributions $\alpha_{\rm S}^n\widetilde{L}^n$; $g^{(3)}$ resums the next-to-next-to-leading logarithmic (NNLL) terms $\alpha_{\rm S}^n\widetilde{L}^{n-1}$, and so forth.

The resummation formulae (2.10), (2.12) and (2.13) can be worked out at any logarithmic accuracy since the functions $\mathcal{H}$ and $\mathcal{G}$ can be expressed (see refs. [38, 39]) in terms of few perturbatively-computable coefficients denoted by $A^{(n)}, B^{(n)}, H^{(n)}, C_N^{(n)}, G_N^{(n)}, \gamma_N^{(n)}$. In the case of the p_T cross section integrated over the rapidity, eq. (2.10) is still valid, provided the double (N_1, N_2)-moments are replaced by the corresponding single N-moments $\mathcal{W}_N, \mathcal{H}_N, \mathcal{G}_N$ (see section 2.2 in ref. [38] and section 2 in ref. [46]).

As discussed in ref. [46], the explicit expressions of the Sudakov exponent $\mathcal{G}^{(N_1,N_2)}$ can be obtained as[3]

$$\mathcal{G}^{(N_1,N_2)} = \frac{1}{2}\left(\mathcal{G}^{(N_1)} + \mathcal{G}^{(N_2)}\right) . \tag{2.14}$$

The first order coefficients $\mathcal{H}_{a_1a_2}^{(N_1,N_2)(1)}$ in the partonic channel $a_1a_2 \to H + X$ are

$$\mathcal{H}_{a_1a_2}^{(N_1,N_2)(1)} = \delta_{ga_2}\left(C_{ga_1,N_1}^{(1)} + \frac{1}{2}\delta_{ga_1}H_g^{(1)}\right) + \delta_{ga_1}\left(C_{ga_2,N_2}^{(1)} + \frac{1}{2}\delta_{ga_2}H_g^{(1)}\right) \tag{2.15}$$

where [40, 50, 51]

$$C_{gg,N}^{(1)} + \frac{1}{2}H_g^{(1)} = \frac{(5+\pi^2)C_A - 3C_F}{4} \qquad C_{gq,N}^{(1)} = \frac{1}{2(N+1)}C_F\,. \tag{2.16}$$

The second order coefficients $\mathcal{H}_{a_1a_2}^{(N_1,N_2)(2)}$ can be written as [48]

$$\begin{aligned}\mathcal{H}_{a_1a_2}^{(N_1,N_2)(2)} = {} & G_{ga_1,N_1}^{(1)}G_{ga_2,N_2}^{(1)} + \left(C_{ga_1,N_1}^{(1)} + \frac{1}{2}\delta_{ga_1}H_g^{(1)}\right)\left(C_{ga_2,N_2}^{(1)} + \frac{1}{2}\delta_{ga_2}H_g^{(1)}\right) \\ & + \delta_{ga_2}C_{ga_1,N_1}^{(2)} + \delta_{ga_1}C_{ga_2,N_2}^{(2)} + \delta_{ga_1}\delta_{ga_2}\left(H_g^{(2)} - \frac{3}{4}\left(H_g^{(1)}\right)^2\right) \\ & + \frac{1}{2}H_g^{(1)}\,\mathcal{H}_{a_1a_2}^{(N_1,N_2)(1)}\end{aligned} \tag{2.17}$$

where $G_{ga,N}^{(1)} = C_a/N/(N-1)$ [39] and the resummation-scheme independent combination on the second line of eq. (2.17) can be obtained by Mellin transformation of eqs. (29), (31) of ref. [48] (equivalently, we can choose a scheme in which $H_g^{(1)} = H_g^{(2)} = 0$ and use eqs. (29), (31) of ref. [48] to evaluate $C_{gq,N}^{(2)}$ and $C_{gg,N}^{(2)}$).

Note that we use the logarithmic variable $\widetilde{L}$ (see eq. (2.11)) to organize the resummation of the large logarithms $\ln(Q^2b^2)$. In the region in which $Qb \gg 1$ we have $\widetilde{L} \sim \ln(Q^2b^2)$ and the use of the variable $\widetilde{L}$ is fully legitimate to arbitrary logarithmic accuracy. When $Qb \ll 1$, we have $\widetilde{L} \to 0$ and $\exp\{\mathcal{G}(\alpha_{\rm S}, \widetilde{L})\} \to 1$. Therefore, the use of $\widetilde{L}$ reduces the effect produced by the resummed contributions in the small-b region (i.e., at large and intermediate values of p_T), where the large-b resummation approach is not justified. In particular, setting $b = 0$ (which corresponds to integrate over the entire p_T range) we

[3] More precisely, this equality is valid in the simplified case where there is a single species of partons (e.g. only gluons). The multiflavour case is illustrated in appendix A of ref. [46].

JHEP06(2012)132

have $\exp\{\mathcal{G}(\alpha_S, \widetilde{L})\} = 1$: this property can be interpreted [38] as a unitarity constraint on the total cross section; transverse-momentum resummation smears the shape of the p_T distribution of the Higgs boson without affecting its total production rate.

The formalism briefly recalled in this section defines a systematic expansion [38] of eq. (2.4): it can be used to obtain predictions that, formally, have uniform perturbative accuracy from the small-p_T region to the large-p_T region. The various orders of this expansion are denoted as NLL+NLO, NNLL+NNLO, etc., where the first label (NLL, NNLL, ...) refers to the logarithmic accuracy at small p_T and the second label (NLO, NNLO, ...) refers to the customary perturbative order for the inclusive cross section.[4] To be precise, the NLL+NLO term of eq. (2.4) is obtained by including the functions $g^{(1)}$, $g^{(2)}$ [36] and the coefficient $\mathcal{H}^{(1)}$ [50, 51] (see eqs. (2.13) and (2.12)) in the resummed component, and by expanding the finite (i.e. large-p_T) component up to $\mathcal{O}(\alpha_S^3)$. At NNLL+NNLO accuracy, the resummed component includes also the function $g_N^{(3)}$ [40] and the coefficient $\mathcal{H}^{(2)}$ [48] (see eqs. (2.13) and (2.12)), while the finite component is expanded up to $\mathcal{O}(\alpha_S^4)$. We point out that the NNLL+NNLO (NLL+NLO) result includes the *full* NNLO (NLO) perturbative contribution, supplemented with the resummation of the logarithmically enhanced terms in the small-p_T region at (N)NLL.

In order implement our calculation in a tool that can be used to perform realistic simulations, it is important to consider the Higgs boson decays. Since we are dealing with a scalar particle, the inclusion of the Higgs decay does not lead to substantial complications. However, the efficient generation of "Higgs events" according to the doubly-differential distribution of eq. (2.4) and the inclusion of the decay are technically non trivial and require substantial improvements in the speed of the numerical program that evaluates the resummed cross section. The finite part in eq. (2.4) is instead evaluated through an appropriate modification of the `HNNLO` code, which being based on the subtraction formalism of ref. [24], is particularly suitable to this purpose.

We recall [38] that, due to our actual definition of the logarithmic parameter $\widetilde{L}$ in eq. (2.10) and to our matching procedure with the perturbative expansion at large p_T, the integral over p_T of the p_T cross section exactly reproduces the customary fixed-order calculation of the total cross section. This integral, however, implies an extrapolation of the resummed result at large transverse momenta, where the resummation cannot improve the accuracy of the fixed order expansion. Moreover, the extrapolation of the resummed cross section at large transverse momenta may lead to unjustified large uncertainties and ensuing lack of predictivity (see section 3 in ref. [38]). This is not a problem if the calculation is limited to the transverse momentum spectrum. In this case, in fact, we can simply use the fixed order result when the uncertainty of the resummed calculation becomes too large. In the present case, since our goal is to generate the full kinematics of the Higgs boson and its decays without a selection on the Higgs transverse momentum, this issue becomes particularly relevant. In the numerical implementation of eq. (2.4) we thus introduce a smooth switching procedure at large p_T, by replacing the resummed cross section in

[4] We note that this notation differs from the one used in refs. [38, 46, 47], where the various terms of the expansion were denoted by NLL+LO, NNLL+NLO and so forth. Since in this paper we do not limit ourselves to study the Higgs p_T spectrum, we prefer to label the fixed order contributions entering the matching procedure according to the order they contribute to the inclusive cross section.

JHEP06(2012)132

eq. (2.4) as follows:

$$\frac{d\hat{\sigma}_{a_1a_2}}{d\hat{y}\,dp_T^2} \to w(p_T)\left(\frac{d\hat{\sigma}^{(\mathrm{res.})}_{a_1a_2}}{d\hat{y}\,dp_T^2}+\frac{d\hat{\sigma}^{(\mathrm{fin.})}_{a_1a_2}}{d\hat{y}\,dp_T^2}\right)+(1-w(p_T))\left[\frac{d\hat{\sigma}_{a_1a_2}}{d\hat{y}\,dp_T^2}\right]_{\mathrm{f.o.}}. \tag{2.18}$$

where the function $w(p_T)$ is defined as[5]

$$w(p_T)=\begin{cases} 1 & p_T \le p_T^{\mathrm{sw.}}-\Delta p_T \\ f(p_T) & p_T^{\mathrm{sw.}}-\Delta p_T < p_T < p_T^{\mathrm{sw.}}+\Delta p_T \\ 0 & p_T \ge p_T^{\mathrm{sw.}}+\Delta p_T \end{cases} \tag{2.19}$$

and the function $f(p_T)$ is chosen in such a way that $w(p_T)$ and $w'(p_T)$ are continuous in all the range of transverse momenta. In particular, we choose

$$f(p_T)=\frac{1}{2}\left(\cos\left(\pi\frac{p_T-(p_T^{\mathrm{sw.}}-\Delta p_T)}{2\Delta p_T}\right)+1\right). \tag{2.20}$$

We have checked that the parameters $p_T^{\mathrm{sw.}}$ and Δp_T can be consistently chosen so as not to spoil our unitarity constraint, and that the integral of our NLL+NLO and NNLL+NNLO resummed result still reproduces well the NLO and NNLO inclusive cross sections (see section 3).

We have implemented our calculation in a numerical program called `HRes`, by considering three decay modes: $H\to\gamma\gamma$, $H\to WW\to l\nu l\nu$ and $H\to ZZ\to 4$ leptons. In the latter case the user can choose between $H\to ZZ\to\mu^+\mu^-e^+e^-$ and $H\to ZZ\to e^+e^-e^+e^-$, which includes the appropriate interference contribution. The program can be downloaded from [45], together with some accompanying notes.

3 Results

3.1 Preliminaries

We consider Higgs boson production at the LHC (e.g. pp collisions at $\sqrt{s}=8\,\mathrm{TeV}$). In order to avoid a multiple presentation of similar results we use MSTW2008 parton distributions [52], with densities and α_S evaluated at each corresponding order, i.e. we use $(n+1)$-loop α_S at N^{n}LL+N^{n}LO and N^{n}LO (with $n=1,2$), and 1-loop α_S for LO. Unless stated otherwise, renormalization, factorization and resummation scales are set to their default values, $\mu_R=\mu_F=2Q=m_H$. We remind the reader that the calculation is performed in the $M_t\to\infty$ limit.

As for the electroweak couplings, we use the scheme where the input parameters are G_F, m_Z, m_W and $\alpha(m_Z)$. In particular we take $G_F=1.16639\times10^{-5}\,\mathrm{GeV}^{-2}$, $m_Z=91.188\,\mathrm{GeV}$, $m_W=80.419\,\mathrm{GeV}$ and $\alpha(m_Z)=1/128.89$. The decay matrix elements are implemented at Born level, i.e., radiative corrections are completely neglected. The Higgs boson is treated in the narrow-width approximation, but in the W and Z decays we take into account finite width effects, by using $\Gamma_W=2.06\,\mathrm{GeV}$ and $\Gamma_Z=2.49\,\mathrm{GeV}$. As explained in section 2, in order to obtain meaningful predictions in the entire range of transverse momenta, we

[5] We note that a simpler switching option is available in the new version of `HqT` [45].

JHEP06(2012)132

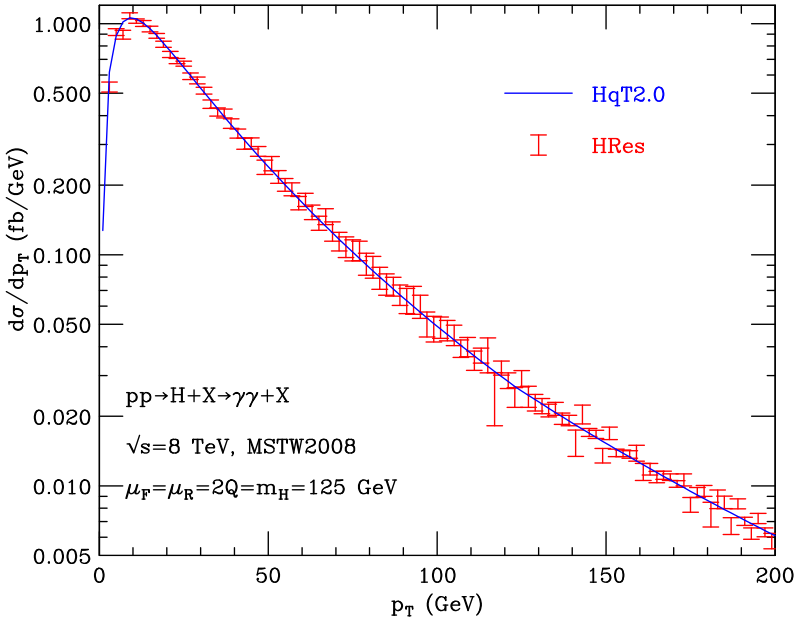

Figure 1. Transverse momentum spectrum for the $H \to \gamma\gamma$ signal at the LHC for $m_H = 125\,\text{GeV}$, obtained at NNLL+NNLO with `HRes` compared to the corresponding result from `HqT`. The result from `HqT` is multiplied by the branching ratio $BR(H \to \gamma\gamma) = 2.245 \times 10^{-3}$ [53].

apply a smooth switching procedure (see eq. (2.18)). In our numerical implementation the parameters in eq. (2.20) are phenomenologically chosen to be $\Delta p_T = 30\,\text{GeV}$ and $p_T^{\text{sw}} = a\,m_H + b(m_H/Q + c)\sqrt{s}$. At NLL+NLO accuracy we set $a = 1/2$, $b = 1.2 \times 10^{-3}$ and $c = 2.5$, whereas at NNLL+NNLO we set $a = 0.6$, $b = 2.8 \times 10^{-3}$ and $c = 0$. We postpone some comments on the dependence of our results on these parameters to section 3.5.

3.2 $H \to \gamma\gamma$

We first consider the production of a SM Higgs boson with mass $m_H = 125\,\text{GeV}$. The width is computed with the program HDECAY [53] to be $\Gamma_H = 4.15\,\text{MeV}$. With this choice of m_H, the effects of finite width can safely be neglected.

When no cuts are applied, the p_T spectrum of the Higgs boson obtained with `HRes` must be in agreement with the one obtained with the `HqT` numerical program. In figure 1 we compare the two spectra to check that this is indeed the case, within the statistical uncertainties. The corresponding inclusive cross sections are reported in table 1[6] , where we show the new resummed results obtained through the `HRes` code, and we compare them with the fixed order predictions obtained with the `HNNLO` code. We see that the NLL+NLO (NNLL+NNLO) inclusive cross section agrees with the NLO (NNLO) result to better than 1%.

As an example, we apply the following cuts on the photons. For each event, we classify the photon transverse momenta according to their minimum and maximum value, $p_{T\,\text{min}}$

[6]Here and in the following the errors in the tables and on the histograms refer to a numerical estimate of the accuracy of the Monte Carlo integration.

JHEP06(2012)132

Cross section	NLO	NLL+NLO	NNLO	NNLL+NNLO
Total [fb]	30.65 ± 0.01	30.79 ± 0.03	38.47 ± 0.15	38.41 ± 0.06
With cuts [fb]	21.53 ± 0.02	21.55 ± 0.01	27.08 ± 0.08	26.96 ± 0.04
Efficiency [%]	70.2	70.0	70.4	70.2

Table 1. Fixed order and resummed cross sections for $pp \to H + X \to \gamma\gamma + X$ at the LHC, before and after geometrical acceptance cuts.

Cross section [fb]	NLO	NLL+NLO	NNLO	NNLL+NNLO
$(2Q = \mu_F = \mu_R) = m_H/2$	25.92 ± 0.02	25.57 ± 0.03	29.52 ± 0.13	29.59 ± 0.11
$(2Q = \mu_F = \mu_R) = m_H$	21.53 ± 0.02	21.55 ± 0.01	27.08 ± 0.08	26.96 ± 0.04
$(2Q = \mu_F = \mu_R) = 2m_H$	18.17 ± 0.01	18.80 ± 0.02	24.43 ± 0.06	24.69 ± 0.06

Table 2. NLO, NLL+NLO, NNLO and NNLL+NNLO accepted cross sections for $pp \to H + X \to \gamma\gamma + X$ at the LHC, for different choices of the scales.

and $p_{T\max}$. The photons are required to be in the central rapidity region, $|\eta| < 2.5$, with $p_{T\min} > 25\,\text{GeV}$ and $p_{T\max} > 40\,\text{GeV}$. Note that an isolation cut on the photons is generally required. For example, a standard isolation is to require the total transverse energy in a cone of a given radius R around each photon to be smaller than a fraction of the photon p_T. Such cuts cannot be taken into account in our resummed calculation, since we are inclusive over the QCD radiation recoiling against the Higgs boson. Their effect can be estimated with the `HNNLO` code and turns out to be rather small.

We recall that the resummation does not affect the total cross section for the Higgs boson production, but when geometrical cuts are applied, their effect can act in a different way on fixed order and resummed calculations. In table 1 we compare the accepted cross sections, obtained by the fixed order and resummed calculations, and the corresponding efficiencies. The numerical errors estimate the statistical uncertainty of the Monte Carlo integration. Comparing resummed and fixed order predictions, we see that there are no substantial differences on the accepted cross section, due to the fact that the integration is performed over a wide kinematical range. In table 2 we report the accepted cross section for different choices of the scales. After selection cuts, the scale uncertainty is about ±15% (±18%) at NLL+NLO (NLO) and ±9% (±10%) at NNLL+NNLO (NNLO).

In figure 2 we study the distribution in the azimuthal separation of the photons in the transverse plane, $\Delta\phi$. At LO the photons are back-to-back, and thus $\Delta\phi$ is 180^o. Beyond LO, events with $\Delta\phi$ different from 180^o are allowed, but NLO (dots) and NNLO (dashes) results show an unphysical behaviour as $\Delta\phi \to 180^o$. The resummed NLL+NLO and NNLL+NNLO results lead instead to a smooth behaviour in this region. On the other hand, $\Delta\phi \to 0$ corresponds to a kinematical configuration where the diphoton system is produced with large transverse momentum, so the result is fully dominated by the corresponding fixed order calculation.

An interesting observable, which has been used by ATLAS to split the $H \to \gamma\gamma$ analysis in categories [54], is the thrust transverse momentum p_{Tt}[7] [55]. Defining the thrust axis $\hat{t}$

[7] In the context of Drell-Yan lepton pair production, this variable is also called a_T [55, 56].

JHEP06(2012)132

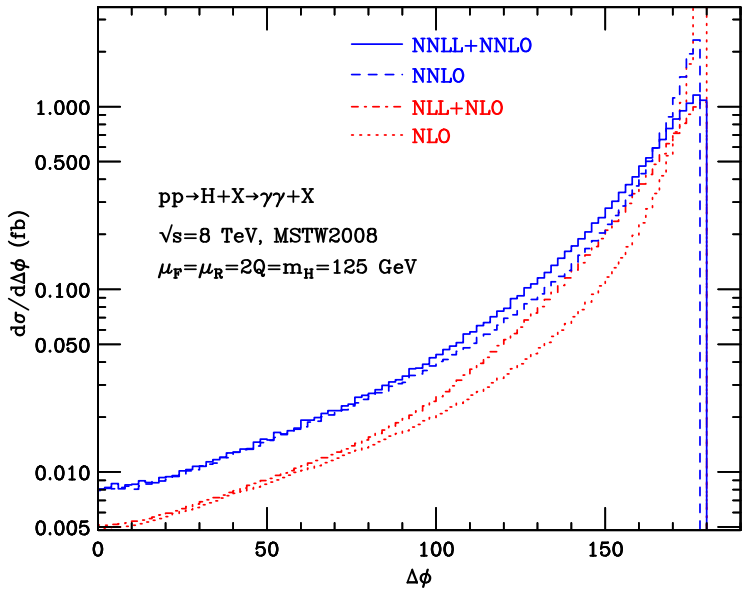

Figure 2. $\Delta\phi$ distribution from the $H \to \gamma\gamma$ signal at the LHC, obtained by the fixed order and resummed calculation.

and the transverse momentum of the diphoton system $\vec{p}_{\rm T}^{\,\gamma\gamma}$ as follows

$$\hat{t} = \frac{\vec{p}_{\rm T}^{\,\gamma_1} - \vec{p}_{\rm T}^{\,\gamma_2}}{|\vec{p}_{\rm T}^{\,\gamma_1} - \vec{p}_{\rm T}^{\,\gamma_2}|}; \;\; \vec{p}_{\rm T}^{\,\gamma\gamma} = \vec{p}_{\rm T}^{\,\gamma_1} + \vec{p}_{\rm T}^{\,\gamma_2}, \tag{3.1}$$

the p_{Tt} is then calculated according to:

$$p_{Tt} = |\vec{p}_{\rm T}^{\,\gamma\gamma} \times \hat{t}|. \tag{3.2}$$

In figure 3 we report the p_{Tt} distribution, obtained at NLO (dots), NNLO (dashes), NLL+NLO (dot dashes) and NNLL+NNLO (solid). We see that in the high p_{Tt} region the NLL+NLO prediction agrees with the NLO one, and the NNLL+NNLO prediction agrees with NNLO. In the low p_{Tt} region the NLO result diverges to $+\infty$, whereas the NNLO diverges to $-\infty$. Such behaviour is analogous to the behaviour of the p_T distribution of the Higgs boson when computed at fixed order in QCD perturbation theory. The NLL+NLO and NNLL+NNLO results obtained with `HRes` are instead finite as $p_{Tt} \to 0$, approaching a constant value.

In figure 4(a), 4(c) we plot the photon p_T distributions $p_{T\rm min}$ and $p_{T\rm max}$. These distributions are enhanced when going from LO to NLO to NNLO according to the increase of the total cross section. We note that, as pointed out in ref. [24], the shape of these distributions sizeable differs when going from LO to NLO and to NNLO. In particular, at the LO the two photons are emitted with the same p_T because the Higgs boson is produced with zero transverse momentum, hence the LO $p_{T\rm min}$ and $p_{T\rm max}$ are exactly identical. Furthermore the LO distribution has a kinematical boundary at $p_T = m_H/2$ (Jacobian peak), which is due to the use of the narrow width approximation. Such condition is released once

JHEP06(2012)132

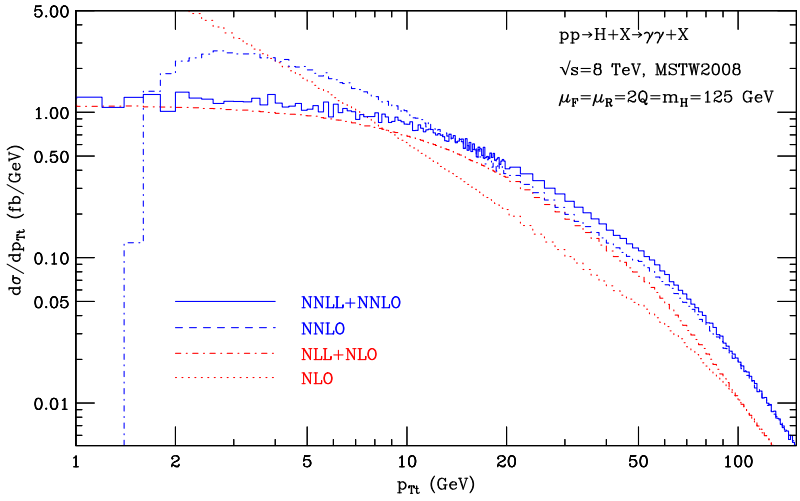

Figure 3. p_{Tt} distribution for the $H \to \gamma\gamma$ signal at the LHC, obtained at NLL+NLO and NNLL+NNLO compared to the corresponding NLO and NNLO results.

extra radiation is accounted for. Thus higher order predictions suffer of perturbative instabilities, i.e. each higher-order perturbative contribution produces (integrable) logarithmic singularities in the vicinity of that boundary, as explained in ref. [57].

The same $p_{T\min}$ and $p_{T\max}$ predictions are shown in figure 4(b), 4(d); in this case the NNLO result is compared with the resummed result at the NLL+NLO and NNLL+NNLO accuracy. As expected [57], resummed results do not suffer of such instabilities in the vicinity of the LO kinematical boundary; the resummed distributions are smooth and the shape is rather stable when going from NLL+NLO to NNLL+NNLO.[8]

An analogous perturbative instability is present in the $p_{T\min}$ distribution around $p_{T\min} \sim 40\,\text{GeV}$ at NLO and NNLO (see figure 4(a)). Such instability, which is not related to the use of the narrow width approximation, is due to the choice of asymmetric cuts for the photons. Beyond LO, the region $p_{T\min} < 40\,\text{GeV}$ opens up, and the step-like behaviour at LO leads to integrable logarithmic singularities at NLO and beyond. The resummed NLL+NLO and NNLL+NNLO results are free of such perturbative instability.

Finally, a variable that is often studied is $\cos\theta^*$, where θ^* is the polar angle of one of the photons with respect to the beam axis in the Higgs boson rest frame. Given the 4-momentum of the photon $p_\gamma = (m_H/2, \vec{p}_T^{\,\gamma}, p_z^\gamma)$ in the Higgs rest frame, the θ^* angle is defined as follows

$$|\cos\theta^*| = \frac{|p_z^\gamma|}{m_H/2}; \tag{3.3}$$

considering the on-shell condition for the photon $p_T^{\gamma\,2} + p_z^{\gamma\,2} = (m_H/2)^2$ and that at the LO

[8] We note that the small-p_T resummation we perform in this paper is not strictly the one needed to cure these logarithmic singularities [57]. Nonetheless, since our resummation provides a correct description of the Higgs boson kinematics, we do not expect that a rigorous treatment of these logarithmic singularities would lead to substantial numerical differences.

JHEP06(2012)132

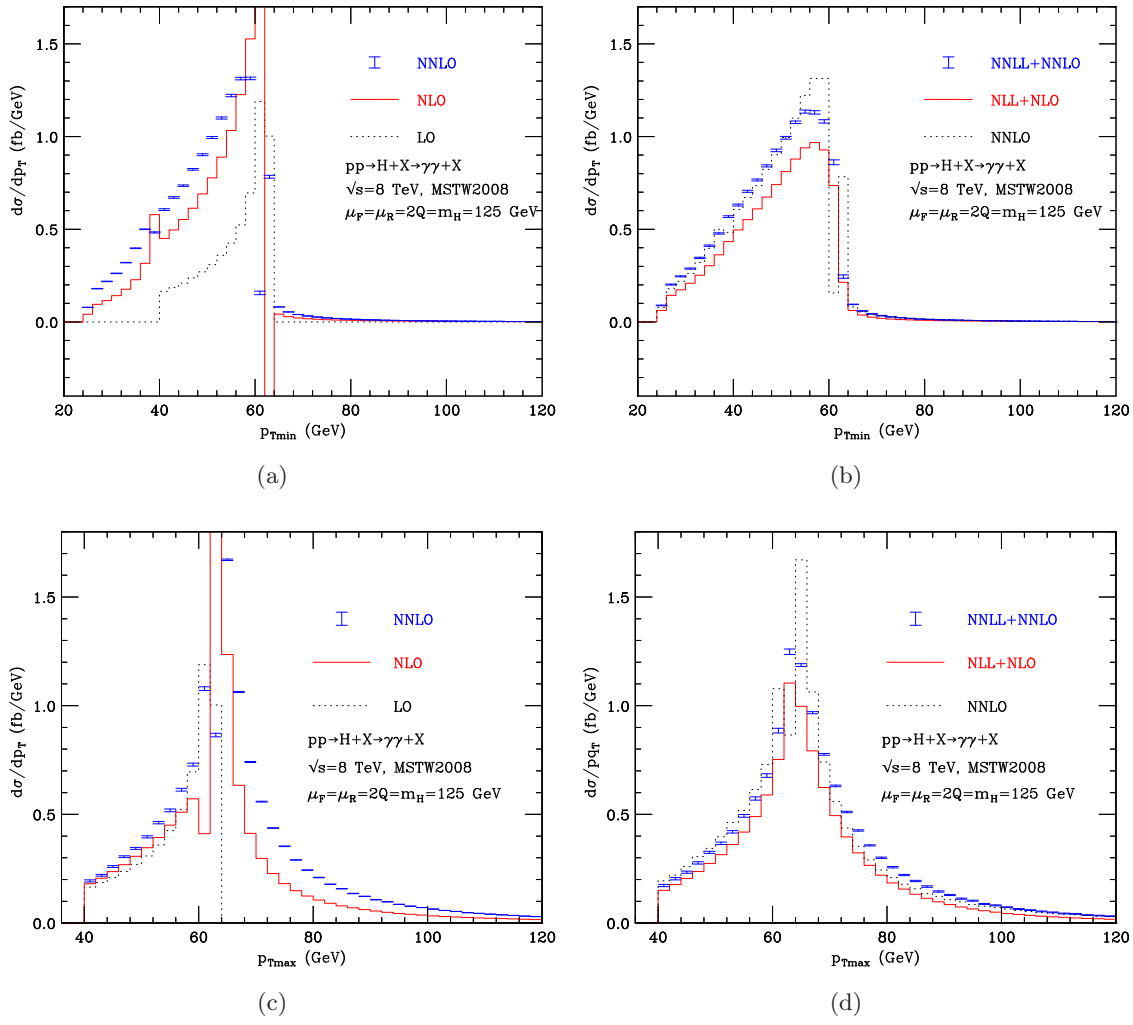

Figure 4. Distributions in $p_{T\min}$ (a,b) and $p_{T\max}$ (c,d) for the $H \to \gamma\gamma$ signal at the LHC, obtained by fixed order (a,c) and resummed (b,d) calculations. In the right panels the fixed order NNLO result is also shown for comparison.

the p_T of the Higgs boson is zero, we can invert the on-shell condition, obtaining

$$|\cos\theta^*| = \sqrt{1 - \frac{4p_T^{\gamma\,2}}{m_H^2}}. \tag{3.4}$$

A cut on the photon transverse momentum p_T^γ implies a maximum value for $\cos\theta^*$ at LO. For example for $m_H = 125\,\text{GeV}$ and $p_T^\gamma \geq 40\,\text{GeV}$ we obtain

$$p_T^\gamma \geq 40\ \text{GeV} \quad \Rightarrow \quad |\cos\theta^*| \leq |\cos\theta^*_{\text{cut}}| \simeq 0.768. \tag{3.5}$$

At the NLO and NNLO the Higgs transverse momentum is non vanishing and events with $|\cos\theta^*| > |\cos\theta^*_{\text{cut}}|$ are kinematically allowed. In the region of the kinematical boundary higher-order perturbative distributions suffer of logarithmic singularities (as it happen for the photon distributions discussed above). In figure 5 we report both the distributions

JHEP06(2012)132

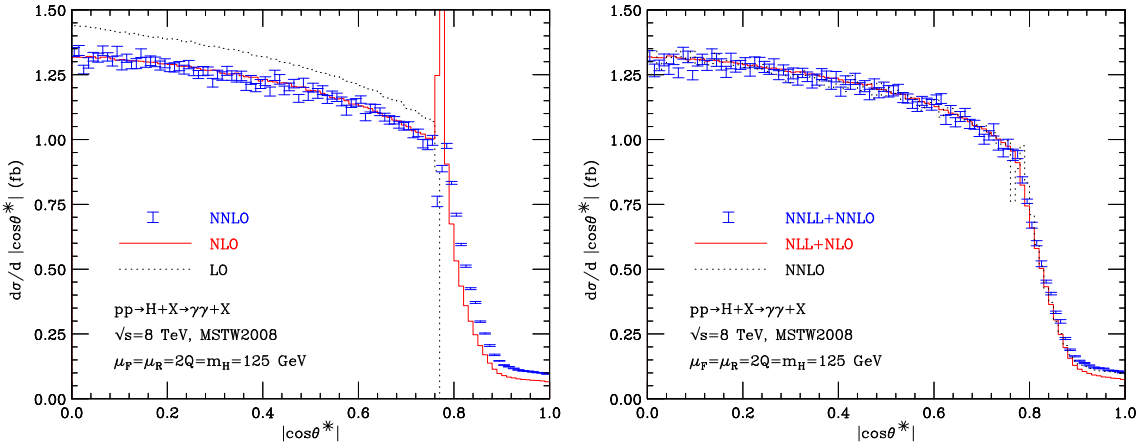

Figure 5. Normalised $\cos\theta^*$ distribution at the LHC. On the left: LO, NLO and NNLO results. On the right: resummed predictions at NLL+NLO and NNLL+NNLO accuracy are compared with the NNLO result.

(normalized to unity) obtained by fixed order and the resummed calculations. We see that the resummed results are smooth in the region around the kinematical boundary. Away from such region, fixed order and resummed results show perfect agreement.

3.3 $H \to WW \to l\nu l\nu$

We now consider the production of a SM Higgs boson with mass $m_H = 140\,\text{GeV}$. The width is computed with the program HDECAY [53] to be $\Gamma_H = 8.11\,\text{MeV}$. We consider the decay $W \to l\nu$ by assuming only one final state lepton combination. In order to isolate the possible signal some acceptance cuts are needed. Here we apply the following set of cuts [58]:

- the event should contain two opposite charged leptons having p_T larger than 20 GeV and in the central rapidity region $|\eta| < 2.5$;
- the missing p_T of the event should be larger than 30 GeV;
- the invariant mass of charged leptons should be larger than 12 GeV.

In table 3 we report the fixed order and resummed predictions for the total and accepted cross section. We see that, also in this case, the inclusion of resummation does not lead to substantial differences on the accepted cross section. In table 4 we report the accepted cross section for different scales. The scale uncertainty is about $\pm 17\%$ at NLL+NLO and NLO, whereas at NNLL+NNLO and NNLO it is reduced to $\pm 10\%$.

For each event, we classify the transverse momenta of the charged leptons according to their minimum and maximum value (as we did for the photon transverse momenta in $H \to \gamma\gamma$). In figure 6 we plot the corresponding distributions. We compare the resummed NLL+NLO and NNLL+NNLO predictions with the corresponding fixed order predictions at the LO, NLO and NNLO accuracy. We see that QCD corrections tend to make the

JHEP06(2012)132

Cross section	NLO	NLL+NLO	NNLO	NNLL+NNLO
Total [fb]	61.58 ± 0.04	61.58 ± 0.04	76.94 ± 0.09	76.88 ± 0.19
With cuts [fb]	20.98 ± 0.03	20.90 ± 0.02	26.44 ± 0.10	26.32 ± 0.05
Efficiency [%]	34.0	33.9	34.4	34.2

Table 3. Fixed order and resummed cross sections for $pp \to H + X \to WW + X \to l\nu l\nu + X$ before and after selection cuts.

Cross section [fb]	NLO	NLL+NLO	NNLO	NNLL+NNLO
$(2Q = \mu_F = \mu_R) = m_H/2$	25.14 ± 0.03	25.13 ± 0.04	29.16 ± 0.17	29.05 ± 0.22
$(2Q = \mu_F = \mu_R) = m_H$	20.98 ± 0.03	20.90 ± 0.02	26.44 ± 0.10	26.32 ± 0.05
$(2Q = \mu_F = \mu_R) = 2m_H$	17.76 ± 0.02	18.26 ± 0.03	23.85 ± 0.07	24.14 ± 0.10

Table 4. Fixed order and resummed accepted cross sections for $pp \to H+X \to WW+X \to l\nu l\nu+X$ at the LHC, for different choices of the scales.

distributions harder. Analogous effects are observed on the average transverse momentum spectrum of the W bosons, which is reported in figure 7. In particular, in order to quantitatively estimate the impact of the resummation, figures 6, 7 are organised in two panels. In the upper panels, we show the predictions obtained by different fixed order and resummed calculations. In the lower panel we plot (in red) the ratio NLL+NLO/NLO and (in blue) NNLL+NNLO/NNLO. From figure 6 we note that, in the peak region, for both the p_{Tmin} and p_{Tmax} distributions, the resummed result is smaller by $5-10\%$ at NLL+NLO and by $2-4\%$ at NNLL+NNLO with respect to the corresponding fixed order prediction. In the intermediate region the resummation affects the results in the opposite direction, enhancing the cross section up to about 30% at NLL+NLO and 10% at NNLL+NNLO. The effects observed for the average p_T of the W bosons (see figure 7) are even more pronounced. These effects on the p_T spectra imply that the agreement between resummed and fixed order predictions we have observed in table 3 cannot persist in general. When more restrictive cuts on the transverse momenta are applied, we anticipate non negligible effects from resummation.

A very important discriminating variable for the $H \to WW \to l\nu l\nu$ decay channel is the azimuthal separation of the charged leptons in the transverse plane, $\Delta\phi$. As is well known [59], for the Higgs boson signal the leptons tend to be close in angle, thus the bulk of the events is produced at small $\Delta\phi$. Our results for the $\Delta\phi$ distribution are reported in figure 8. We can see that in the very small $\Delta\phi$ region ($\Delta\phi \lesssim 30^o$), there are less events than expected: this is an effect of the applied cuts. We notice that the steepness of the distributions increases when going from LO to NLO and from NLO to NNLO, and also increases when going from fixed order to resummed predictions, i.e. from NLO to NLL+NLO and from NNLO to NNLL+NNLO. This fact can be interpreted as follows: when the Higgs boson p_T distribution is harder the final state leptons tend to be more boosted in the transverse plane and thus their transverse angular separation becomes smaller. As a consequence the steepness of the $\Delta\phi$ distribution increases and the efficiency of cuts slightly increases with the perturbative accuracy.

JHEP06(2012)132

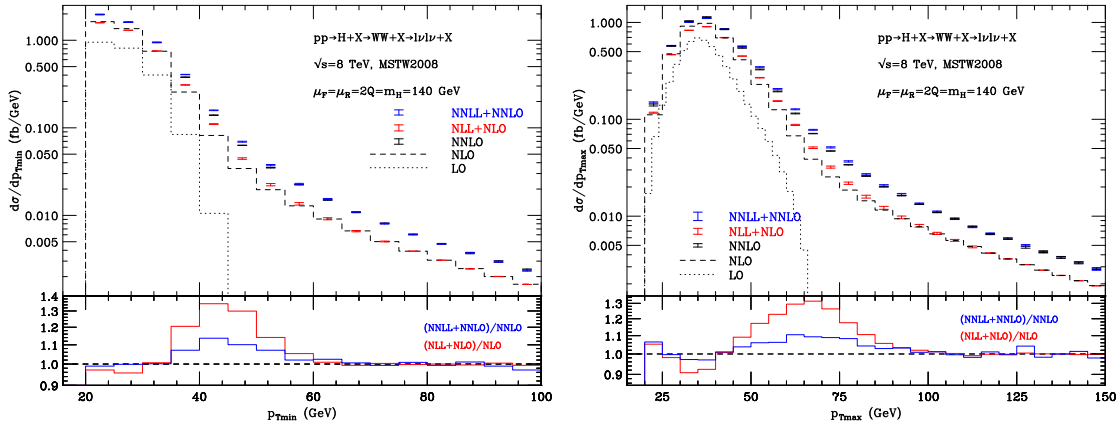

Figure 6. Transverse momentum spectra of the lepton with minimum (left) and maximum (right) p_T for $pp \to H + X \to WW + X \to l\nu l\nu + X$ at the LHC. Resummed results at NLL+NLO and NNLL+NNLO accuracy are compared with fixed order predictions at LO, NLO and NNLO. The lower panels show the NNLL+NNLO result normalized to NNLO (solid) and the NLL+NLO result normalized to NLO (dashes).

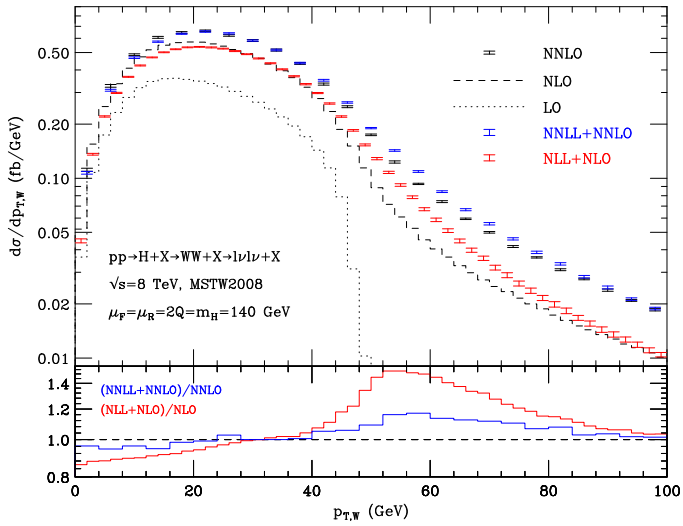

Figure 7. Average transverse momentum spectrum of the W bosons for $pp \to H+X \to WW+X \to l\nu l\nu + X$ at the LHC when cuts are applied. Resummed results at NLL+NLO and NNLL+NNLO accuracy are compared with fixed order predictions at LO, NLO and NNLO. The lower panel shows the NNLL+NNLO result normalized to NNLO (solid) and the NLL+NLO result normalized to NLO (dashes).

3.4 $H \to ZZ \to \mu^+\mu^- e^+e^-$

We now consider the production of a Higgs boson with mass $m_H = 150\,\text{GeV}$. The width is computed with the program HDECAY [53] to be $\Gamma_H = 16.9\,\text{MeV}$. In this mass region, the $H \to ZZ \to 4l$ decay mode is not the dominant decay channel, but still it can provide a clean and useful four lepton signature. In the following we consider the decay of the Higgs boson in two different lepton pairs.

JHEP06(2012)132

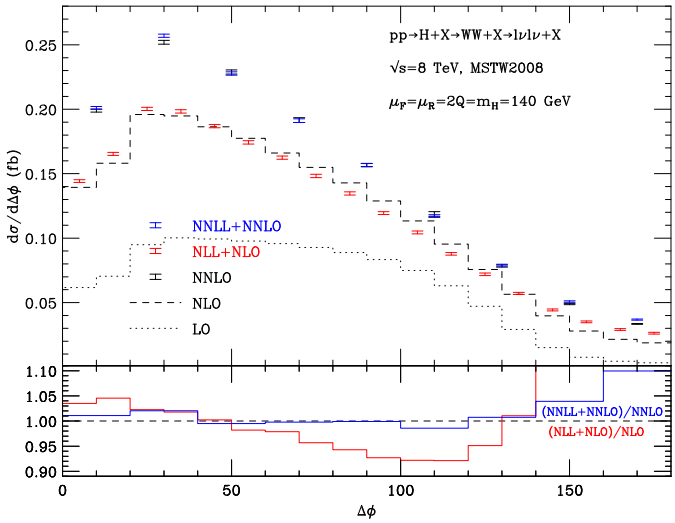

Figure 8. Same as in figure 7 but for the $\Delta\phi$ distribution.

We consider the following cuts [58]:

- the event should contain two pairs of opposite charged leptons
- each lepton must have p_T larger than 5 GeV and should be in the central rapidity region $|\eta| < 2.5$;
- for each lepton pair, the invariant mass closest (m_1) and next-to-closest (m_2) to m_Z are found; then m_1, m_2 are required to be $m_1 > 50$ GeV and $m_2 > 12$ GeV.

Note that an isolation cut on the leptons is generally required. For example, a typical isolation is to require the total transverse energy E_T in a cone of a given radius R around each lepton to be smaller than a fraction of the lepton p_T. As in the $H \to \gamma\gamma$ decay mode isolation cuts cannot be applied, because in the resummed calculation we are necessarily inclusive over the QCD radiation accompanying the Higgs boson. By using the fixed order `HNNLO` code we have checked that the numerical effect of the isolation cuts is extremely small.

In table 5 we compare the effects of cuts on the inclusive cross sections. As in the $H \to \gamma\gamma$ and $H \to WW$ decays, the efficiency slightly improves increasing the perturbative accuracy, but no substantial effects from resummation are observed. In table 6 the accepted cross section for different choices of the scales is reported. At the NLL+NLO (NLO) accuracy the ensuing scale uncertainty is $\sim \pm 15\%$ ($\pm 17\%$) and at the NNLL+NNLO (NNLO) it is $\sim \pm 9\%$ ($\pm 10\%$).

In figure 9 we plot the four p_T spectra of the final state leptons. Note that at LO the p_{T1}, p_{T2} are kinematically bounded by $m_H/2$, whereas $p_{T3} < m_H/3$ and $p_{T4} < m_H/4$. In the vicinity of such boundaries, higher order QCD predictions may in principle develop perturbative instabilities. On the other hand, contrary to what happens in the $H \to \gamma\gamma$ decay mode, the LO distributions smoothly reach their kinematical boundary and we do not

JHEP06(2012)132

Cross section	NLO	NLL+NLO	NNLO	NNLL+NNLO
Total [fb]	1.720 ± 0.001	1.720 ± 0.002	2.142 ± 0.004	2.156 ± 0.006
With cuts [fb]	1.127 ± 0.001	1.136 ± 0.001	1.413 ± 0.005	1.427 ± 0.003
Efficiency [%]	65.6	66.0	66.0	66.2

Table 5. Fixed order and resummed cross section for $pp \to H + X \to ZZ + X \to \mu^+\mu^- e^+ e^- + X$ cross section before and after geometrical acceptance cuts.

Cross section [fb]	NLO	NLL+NLO	NNLO	NNLL+NNLO
$(2Q = \mu_F = \mu_R) = m_H/2$	1.350 ± 0.001	1.350 ± 0.004	1.572 ± 0.007	1.570 ± 0.006
$(2Q = \mu_F = \mu_R) = m_H$	1.127 ± 0.001	1.136 ± 0.001	1.413 ± 0.005	1.427 ± 0.003
$(2Q = \mu_F = \mu_R) = 2m_H$	0.954 ± 0.001	0.992 ± 0.003	1.273 ± 0.003	1.310 ± 0.003

Table 6. Fixed order and resummed accepted cross sections for $pp \to H + X \to ZZ + X \to \mu^+\mu^- e^+ e^- + X$ at the LHC, for different choices of the scales.

observe perturbative instabilities beyond the LO. The impact of resummation is to make the transverse momentum spectra harder. The resummation effects are more pronounced in the leading lepton transverse momentum spectrum (see figure 9(a)) and less evident in the softest lepton spectrum (see figure 9(d)).

In figure 10 we show the average p_T distribution of the two Z bosons. The comments are analogous to those for previous distributions: QCD radiation tends to make the distribution harder and the fixed order results are again recovered at large transverse momentum.

3.5 Discussion

The predictions we have presented in this paper are obtained within a purely perturbative framework. It is well known that the transverse-momentum distribution is affected by Non Perturbative (NP) effects, which become important as p_T becomes small. A way of modelling these effects is to introduce an NP transverse-momentum smearing of the distribution. In the case of resummed calculations in impact parameter space, the NP smearing is implemented by multiplying the b-space perturbative form factor by an NP form factor. A possible form for the NP form factor is a gaussian smearing $S_{NP} = \exp\{-gb^2\}$.

The quantitative effect of this smearing factor on the p_T spectrum has been studied in refs. [38, 47], where the parameter g was varied in the range suggested by the study of ref. [66]. The results of refs. [38, 47] show that the NP effects on the spectrum are quantitatively relevant only in the very small p_T region. By modifying the shape of the p_T spectrum, the inclusion of NP effects indirectly affects also the other kinematical distributions studied in this paper. For example, we find that in the p_{Tt} distribution studied in figure 3, the value of the differential cross section $d\sigma/dp_{Tt}$ as $p_{Tt} \to 0$ is affected by about $2 - 5\%$ by NP effects. In the case of the $\Delta\phi$ distribution in figure 2 the NP effects affect the high $\Delta\phi$ region by about $1 - 2\%$. The effects on other distributions are generally of the same order or smaller.

JHEP06(2012)132

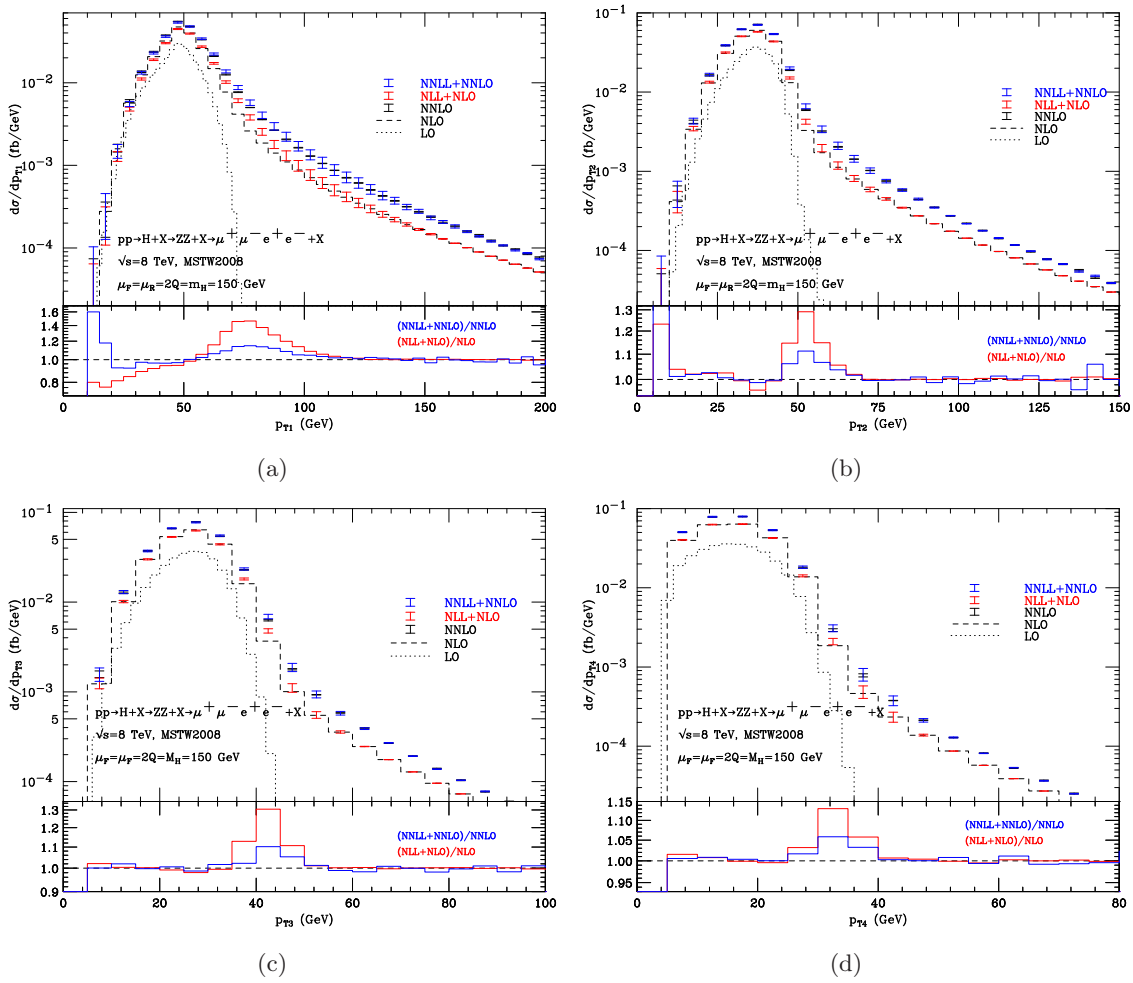

Figure 9. Transverse momentum spectra of the final state leptons for $pp \to H + X \to ZZ + X \to \mu^+\mu^- e^+ e^- + X$ at the LHC, when cuts are applied. The lepton p_T are ordered according to decreasing p_T. They are obtained through fixed order (black) and resummed (red and blue) calculations. The lower panels show the ratios between resummed and fixed order predictions.

As explained at the end of section 2 our numerical program implements a smooth switching procedure between the resummed and fixed order results (see eqs. (2.18) and (2.20)). The numerical parameters in eq. (2.18) can be consistently chosen such that the integral of our NLL+NLO and NNLL+NNLO resummed result still reproduces well the NLO and NNLO inclusive cross sections. It is interesting to study the uncertainty inherent in such switching procedure. In figure 11 we show the impact of different switching functions $w(p_T)$ (see eq. (2.19)) on the NNLL+NNLO normalized p_T spectrum of a Higgs boson with $m_H = 125\,\text{GeV}$. In the left panel the default choice of $w(p_T)$ (blue curve) is compared to the corresponding functions obtained by shifting $p_T^{\text{SW}\cdot}$ by $\pm 20\,\text{GeV}$ (red, magenta curves), or by using $\Delta p_T = 20\,\text{GeV}$ (green curve). We see that the relative effect with respect to the default choice adopted in `HRes` (right panel) is rather small, being at most 3%, thus well within the scale uncertainties (see e.g. figure 4 of ref. [47]). We also

JHEP06(2012)132

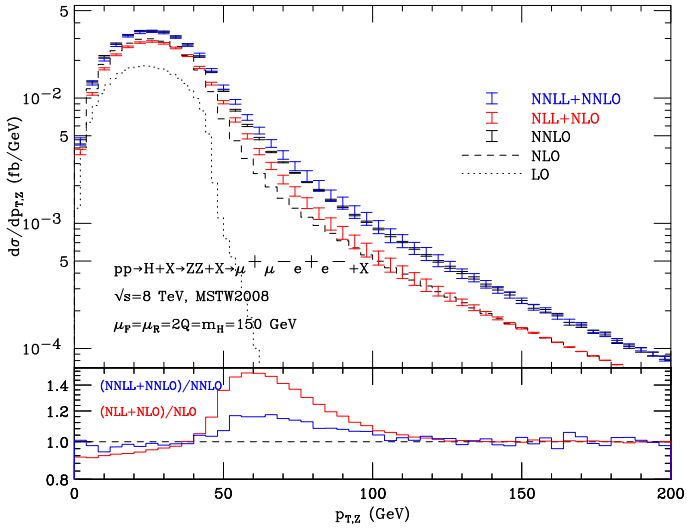

Figure 10. Average p_T spectrum of the Z bosons for $pp \to H + X \to ZZ + X \to \mu^+\mu^- e^+ e^- + X$ at the LHC, when cuts are applied. Resummed results at NLL+NLO and NNLL+NNLO accuracy are compared with fixed order predictions at LO, NLO and NNLO. The lower panel shows the NNLL+NNLO result normalized to NNLO (solid) and the NLL+NLO result normalized to NLO (dashes).

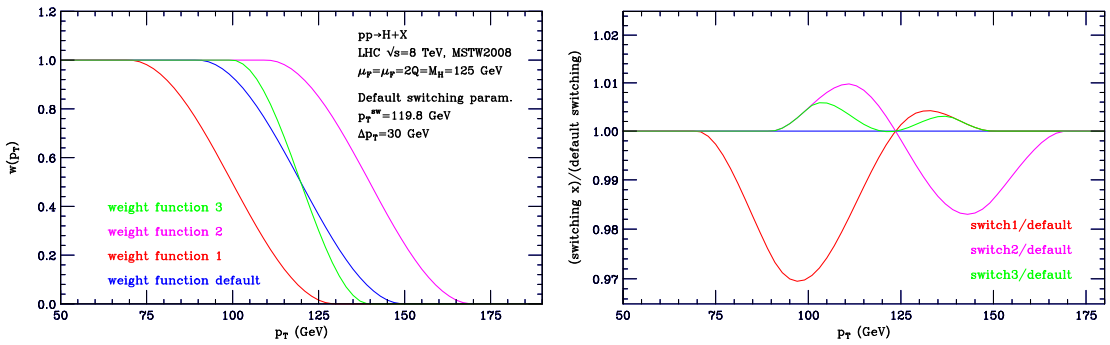

(a) (b)

Figure 11. Effects of different switching procedures on the Higgs p_T distribution. Switching functions $w(p_T)$ (left panel). Relative effects on the standard result from `HRes` (right panel).

stress that the effects of the different switching procedures on the total cross section is completely negligible.

We conclude this section by adding few comments on the work of ref. [60]. In this paper the RESBOS generator [61], which is based on the classical b-space resummation formalism of ref. [32], is used to perform a study of transverse momentum resummation effects in the $H \to WW \to l\nu l\nu$ and $H \to ZZ \to 4l$ channels at the Tevatron and the LHC. The resummed calculation in the low p_T region is matched to the $\mathcal{O}(\alpha_S^3)$ result at high p_T. Besides the differences in the resummation formalism (see ref. [38] for a detailed discussion) there are a few differences with respect to the work presented here.

JHEP06(2012)132

Our calculation implements the value of the coefficient $A^{(3)}$ from ref. [49], whereas in ref. [60] the authors use the result of ref. [62] that applies to threshold resummation. The calculation of ref. [60] does not include the hard collinear coefficients $\mathcal{H}^{(2)}$ presented in ref. [48] and thus its accuracy, with our notations, is essentially limited to NLL+NLO (plus some of the NNLL terms). Finally, the calculation of ref. [60] does not exploit a unitarity constraint on the total cross section, and thus the normalization of the ensuing resummed spectra is not constrained.

In their phenomenological study, when comparing resummed and fixed-order NLO predictions, the authors of ref. [60] find significant resummation effects. The reason is twofold. First, the cuts that are considered in ref. [60] are more restrictive, and thus resummation effects are made more relevant. Second, the comparison is done one order lower than ours (i.e. the NLL+NLO resummed prediction is compared to the fixed order NLO result) where we also find more significant distortions of the relevant kinematical distributions (see figures 6–10).

4 Summary and outlook

We have presented a calculation of the NNLL+NNLO cross section for Higgs boson production at the LHC, in the decay modes $H \to \gamma\gamma$, $H \to WW \to l\nu l\nu$ and $H \to ZZ \to 4$ leptons. The calculation takes into account some illustrative experimental cuts analogous to the ones designed to isolate the Higgs boson signal.

Our calculation is implemented in the numerical program `HRes` [45]. The present version of the program includes the most relevant decay modes of the Higgs boson, namely, $H \to \gamma\gamma$, $H \to WW \to l\nu l\nu$ and $H \to ZZ \to 4$ leptons. In the latter case it is possible to choose between $H \to ZZ \to \mu^+\mu^- e^+ e^-$ and $H \to ZZ \to e^+e^-e^+e^-$, which includes the appropriate interference contribution. The user can apply all the required cuts on the Higgs boson and its decay products and plot the corresponding distributions in the form of bin histograms. These features should make our program a useful tool for Higgs searches and studies at the Tevatron and the LHC.

The calculations performed through `HRes` strictly implement the large M_t approximation. This is known to be a good approximation for the p_T spectrum of the Higgs boson, provided that p_T is not too large ($p_T \lesssim M_t$) [63]. For very large transverse momenta the large-M_t approximation is bound to fail, since the QCD radiation accompanying the Higgs boson becomes sensitive to the heavy-quark loop. The inclusion of top and bottom mass effects up to $\mathcal{O}(\alpha_S^3)$ in `HRes` is feasible and is left to future work. Another limitation of the calculation is that we completely neglect radiative corrections in the Higgs boson decay. The full QCD+EW corrections to the decay modes $H \to WW(ZZ) \to 4$ leptons are available [64, 65] and we plan to include these effects in a future version of the program.

We have stressed that our calculation is inclusive over the accompanying QCD radiation. For some applications, as for instance, studies in the $H \to WW$ decay channel, a jet veto is necessary, and thus `HRes` may not be the right tool for such studies. We note that, after the completion of this work a paper appeared [67] where the resummation for the jet veto efficiency has been carried out up to NLL+NNLO. Such results are in some respects complementary to those presented here.

JHEP06(2012)132

Acknowledgments

We wish to thank Stefano Catani for many helpful discussions and comments on the manuscript. This work was supported in part by UBACYT, CONICET, ANPCyT, INFN and the Research Executive Agency (REA) of the European Union under the Grant Agreement number PITN-GA-2010-264564 (LHCPhenoNet). We thank the Galileo Galilei Institute for Theoretical Physics for the hospitality during the completion of this work.

References

[1] F. Englert and R. Brout, *Broken symmetry and the mass of gauge vector mesons*, *Phys. Rev. Lett.* **13** (1964) 321 [INSPIRE].

[2] P.W. Higgs, *Broken symmetries, massless particles and gauge fields*, *Phys. Lett.* **12** (1964) 132 [INSPIRE].

[3] P.W. Higgs, *Broken symmetries and the masses of gauge bosons*, *Phys. Rev. Lett.* **13** (1964) 508 [INSPIRE].

[4] ATLAS collaboration, G. Aad et al., *Combined search for the standard model Higgs boson using up to* 4.9 fb^{-1} *of pp collision data at* $\sqrt{s} = 7$ *TeV with the ATLAS detector at the LHC*, *Phys. Lett.* **B 710** (2012) 49 [arXiv:1202.1408] [INSPIRE].

[5] CMS collaboration, S. Chatrchyan et al., *Combined results of searches for the standard model Higgs boson in pp collisions at* $\sqrt{s} = 7$ *TeV*, *Phys. Lett.* **B 710** (2012) 26 [arXiv:1202.1488] [INSPIRE].

[6] TEVNPH, CDF, and D0 collaborations, *Combined CDF and D0 search for standard model Higgs boson production with up to* 10 fb^{-1} *of data*, arXiv:1203.3774 [FERMILAB-CONF-12-065-E] [INSPIRE].

[7] H. Georgi, S. Glashow, M. Machacek and D.V. Nanopoulos, *Higgs bosons from two gluon annihilation in proton proton collisions*, *Phys. Rev. Lett.* **40** (1978) 692 [INSPIRE].

[8] S. Dawson, *Radiative corrections to Higgs boson production*, *Nucl. Phys.* **B 359** (1991) 283 [INSPIRE].

[9] A. Djouadi, M. Spira and P. Zerwas, *Production of Higgs bosons in proton colliders: QCD corrections*, *Phys. Lett.* **B 264** (1991) 440 [INSPIRE].

[10] M. Spira, A. Djouadi, D. Graudenz and P. Zerwas, *Higgs boson production at the LHC*, *Nucl. Phys.* **B 453** (1995) 17 [hep-ph/9504378] [INSPIRE].

[11] R.V. Harlander and W.B. Kilgore, *Next-to-next-to-leading order Higgs production at hadron colliders*, *Phys. Rev. Lett.* **88** (2002) 201801 [hep-ph/0201206] [INSPIRE].

[12] C. Anastasiou and K. Melnikov, *Higgs boson production at hadron colliders in NNLO QCD*, *Nucl. Phys.* **B 646** (2002) 220 [hep-ph/0207004] [INSPIRE].

[13] V. Ravindran, J. Smith and W.L. van Neerven, *NNLO corrections to the total cross-section for Higgs boson production in hadron hadron collisions*, *Nucl. Phys.* **B 665** (2003) 325 [hep-ph/0302135] [INSPIRE].

[14] S. Marzani, R.D. Ball, V. Del Duca, S. Forte and A. Vicini, *Higgs production via gluon-gluon fusion with finite top mass beyond next-to-leading order*, *Nucl. Phys.* **B 800** (2008) 127 [arXiv:0801.2544] [INSPIRE].

JHEP06(2012)132

[15] R.V. Harlander and K.J. Ozeren, *Top mass effects in Higgs production at next-to-next-to-leading order QCD: virtual corrections*, *Phys. Lett.* **B 679** (2009) 467 [arXiv:0907.2997] [INSPIRE].

[16] R.V. Harlander and K.J. Ozeren, *Finite top mass effects for hadronic Higgs production at next-to-next-to-leading order*, *JHEP* **11** (2009) 088 [arXiv:0909.3420] [INSPIRE].

[17] R.V. Harlander, H. Mantler, S. Marzani and K.J. Ozeren, *Higgs production in gluon fusion at next-to-next-to-leading order QCD for finite top mass*, *Eur. Phys. J.* **C 66** (2010) 359 [arXiv:0912.2104] [INSPIRE].

[18] A. Pak, M. Rogal and M. Steinhauser, *Virtual three-loop corrections to Higgs boson production in gluon fusion for finite top quark mass*, *Phys. Lett.* **B 679** (2009) 473 [arXiv:0907.2998] [INSPIRE].

[19] A. Pak, M. Rogal and M. Steinhauser, *Finite top quark mass effects in NNLO Higgs boson production at LHC*, *JHEP* **02** (2010) 025 [arXiv:0911.4662] [INSPIRE].

[20] S. Catani, D. de Florian and M. Grazzini, *Direct Higgs production and jet veto at the Tevatron and the LHC in NNLO QCD*, *JHEP* **01** (2002) 015 [hep-ph/0111164] [INSPIRE].

[21] C. Anastasiou, K. Melnikov and F. Petriello, *Higgs boson production at hadron colliders: differential cross sections through next-to-next-to-leading order*, *Phys. Rev. Lett.* **93** (2004) 262002 [hep-ph/0409088] [INSPIRE].

[22] C. Anastasiou, K. Melnikov and F. Petriello, *Fully differential Higgs boson production and the di-photon signal through next-to-next-to-leading order*, *Nucl. Phys.* **B 724** (2005) 197 [hep-ph/0501130] [INSPIRE].

[23] C. Anastasiou, G. Dissertori and F. Stockli, *NNLO QCD predictions for the $H \to WW \to l\nu l\nu$ signal at the LHC*, *JHEP* **09** (2007) 018 [arXiv:0707.2373] [INSPIRE].

[24] S. Catani and M. Grazzini, *An NNLO subtraction formalism in hadron collisions and its application to Higgs boson production at the LHC*, *Phys. Rev. Lett.* **98** (2007) 222002 [hep-ph/0703012] [INSPIRE].

[25] M. Grazzini, *NNLO predictions for the Higgs boson signal in the $H \to WW \to l\nu l\nu$ and $H \to ZZ \to 4l$ decay channels*, *JHEP* **02** (2008) 043 [arXiv:0801.3232] [INSPIRE].

[26] Y.L. Dokshitzer, D. Diakonov and S. Troian, *On the transverse momentum distribution of massive lepton pairs*, *Phys. Lett.* **B 79** (1978) 269 [INSPIRE].

[27] Y.L. Dokshitzer, D. Diakonov and S. Troian, *Hard processes in quantum chromodynamics*, *Phys. Rep.* **58** (1980) 269.

[28] G. Parisi and R. Petronzio, *Small transverse momentum distributions in hard processes*, *Nucl. Phys.* **B 154** (1979) 427 [INSPIRE].

[29] G. Curci, M. Greco and Y. Srivastava, *QCD jets from coherent states*, *Nucl. Phys.* **B 159** (1979) 451 [INSPIRE].

[30] J.C. Collins and D.E. Soper, *Back-to-back jets in QCD*, *Nucl. Phys.* **B 193** (1981) 381 [*Erratum ibid.* **B 213** (1983) 545] [INSPIRE].

[31] J.C. Collins and D.E. Soper, *Back-to-back jets: Fourier transform from B to K-transverse*, *Nucl. Phys.* **B 197** (1982) 446 [INSPIRE].

[32] J.C. Collins, D.E. Soper and G.F. Sterman, *Transverse momentum distribution in Drell-Yan pair and W and Z boson production*, *Nucl. Phys.* **B 250** (1985) 199 [INSPIRE].

JHEP06(2012)132

[33] J. Kodaira and L. Trentadue, *Summing soft emission in QCD*, *Phys. Lett.* **B 112** (1982) 66 [INSPIRE].

[34] J. Kodaira and L. Trentadue, *Soft gluon effects in perturbative quantum chromodynamics*, SLAC-PUB-2934 (1982).

[35] J. Kodaira and L. Trentadue, *Single logarithm effects in electron-positron annihilation*, *Phys. Lett.* **B 123** (1983) 335 [INSPIRE].

[36] S. Catani, E. D'Emilio and L. Trentadue, *The gluon form-factor to higher orders: gluon gluon annihilation at small Q-transverse*, *Phys. Lett.* **B 211** (1988) 335 [INSPIRE].

[37] S. Catani, D. de Florian and M. Grazzini, *Universality of nonleading logarithmic contributions in transverse momentum distributions*, *Nucl. Phys.* **B 596** (2001) 299 [hep-ph/0008184] [INSPIRE].

[38] G. Bozzi, S. Catani, D. de Florian and M. Grazzini, *Transverse-momentum resummation and the spectrum of the Higgs boson at the LHC*, *Nucl. Phys.* **B 737** (2006) 73 [hep-ph/0508068] [INSPIRE].

[39] S. Catani and M. Grazzini, *QCD transverse-momentum resummation in gluon fusion processes*, *Nucl. Phys.* **B 845** (2011) 297 [arXiv:1011.3918] [INSPIRE].

[40] D. de Florian and M. Grazzini, *Next-to-next-to-leading logarithmic corrections at small transverse momentum in hadronic collisions*, *Phys. Rev. Lett.* **85** (2000) 4678 [hep-ph/0008152] [INSPIRE].

[41] D. de Florian and M. Grazzini, *The structure of large logarithmic corrections at small transverse momentum in hadronic collisions*, *Nucl. Phys.* **B 616** (2001) 247 [hep-ph/0108273] [INSPIRE].

[42] D. de Florian, M. Grazzini and Z. Kunszt, *Higgs production with large transverse momentum in hadronic collisions at next-to-leading order*, *Phys. Rev. Lett.* **82** (1999) 5209 [hep-ph/9902483] [INSPIRE].

[43] V. Ravindran, J. Smith and W. Van Neerven, *Next-to-leading order QCD corrections to differential distributions of Higgs boson production in hadron hadron collisions*, *Nucl. Phys.* **B 634** (2002) 247 [hep-ph/0201114] [INSPIRE].

[44] C.J. Glosser and C.R. Schmidt, *Next-to-leading corrections to the Higgs boson transverse momentum spectrum in gluon fusion*, *JHEP* **12** (2002) 016 [hep-ph/0209248] [INSPIRE].

[45] M. Grazzini, *Higgs production at hadron colliders: tools*, http://theory.fi.infn.it/grazzini/codes.html.

[46] G. Bozzi, S. Catani, D. de Florian and M. Grazzini, *Higgs boson production at the LHC: transverse-momentum resummation and rapidity dependence*, *Nucl. Phys.* **B 791** (2008) 1 [arXiv:0705.3887] [INSPIRE].

[47] D. de Florian, G. Ferrera, M. Grazzini and D. Tommasini, *Transverse-momentum resummation: Higgs boson production at the Tevatron and the LHC*, *JHEP* **11** (2011) 064 [arXiv:1109.2109] [INSPIRE].

[48] S. Catani and M. Grazzini, *Higgs boson production at hadron colliders: hard-collinear coefficients at the NNLO*, ZU-TH-12-11 (2012).

[49] T. Becher and M. Neubert, *Drell-Yan production at small q_T, transverse parton distributions and the collinear anomaly*, *Eur. Phys. J.* **C 71** (2011) 1665 [arXiv:1007.4005] [INSPIRE].

JHEP06(2012)132

[50] R. Kauffman, *Higher order corrections to Higgs boson p_T*, *Phys. Rev.* **D 45** (1992) 1512 [INSPIRE].

[51] C. Yuan, *Kinematics of the Higgs boson at hadron colliders: NLO QCD gluon resummation*, *Phys. Lett.* **B 283** (1992) 395 [INSPIRE].

[52] A. Martin, W. Stirling, R. Thorne and G. Watt, *Parton distributions for the LHC*, *Eur. Phys. J.* **C 63** (2009) 189 [arXiv:0901.0002] [INSPIRE].

[53] A. Djouadi, J. Kalinowski and M. Spira, *HDECAY: a program for Higgs boson decays in the standard model and its supersymmetric extension*, *Comput. Phys. Commun.* **108** (1998) 56 [hep-ph/9704448] [INSPIRE].

[54] ATLAS collaboration, G. Aad et al., *Search for the standard model Higgs boson in the diphoton decay channel with* 4.9 fb^{-1} *ofpp collisions at* $\sqrt{s} = 7$ *TeV with ATLAS*, *Phys. Rev. Lett.* **108** (2012) 111803 [arXiv:1202.1414] [INSPIRE].

[55] M. Vesterinen and T. Wyatt, *A novel technique for studying the Z boson transverse momentum distribution at hadron colliders*, *Nucl. Instrum. Meth.* **A 602** (2009) 432 [arXiv:0807.4956] [INSPIRE].

[56] A. Banfi, M. Dasgupta and R.M. Duran Delgado, *The $a(T)$ distribution of the Z boson at hadron colliders*, *JHEP* **12** (2009) 022 [arXiv:0909.5327] [INSPIRE].

[57] S. Catani and B. Webber, *Infrared safe but infinite: soft gluon divergences inside the physical region*, *JHEP* **10** (1997) 005 [hep-ph/9710333] [INSPIRE].

[58] S. Dittmaier et al., *Handbook of LHC Higgs cross sections:* 2. *Differential distributions*, arXiv:1201.3084 [INSPIRE].

[59] M. Dittmar and H.K. Dreiner, *How to find a Higgs boson with a mass between* 155 *GeV*–180 *GeV at the LHC*, *Phys. Rev.* **D 55** (1997) 167 [hep-ph/9608317] [INSPIRE].

[60] Q.-H. Cao and C.-R. Chen, *Resummation effects in the search of SM Higgs boson at hadron colliders*, *Phys. Rev.* **D 76** (2007) 073006 [arXiv:0704.1344] [INSPIRE].

[61] C. Balázs and C. Yuan, *Higgs boson production at the LHC with soft gluon effects*, *Phys. Lett.* **B 478** (2000) 192 [hep-ph/0001103] [INSPIRE].

[62] S. Moch, J. Vermaseren and A. Vogt, *The three loop splitting functions in QCD: the nonsinglet case*, *Nucl. Phys.* **B 688** (2004) 101 [hep-ph/0403192] [INSPIRE].

[63] U. Baur and E.N. Glover, *Higgs boson production at large transverse momentum in hadronic collisions*, *Nucl. Phys.* **B 339** (1990) 38 [INSPIRE].

[64] A. Bredenstein, A. Denner, S. Dittmaier and M. Weber, *Precise predictions for the Higgs-boson decay $H \to WW/ZZ \to 4$ leptons*, *Phys. Rev.* **D 74** (2006) 013004 [hep-ph/0604011] [INSPIRE].

[65] A. Bredenstein, A. Denner, S. Dittmaier and M. Weber, *Radiative corrections to the semileptonic and hadronic Higgs-boson decays $H \to WW/ZZ \to 4$ fermions*, *JHEP* **02** (2007) 080 [hep-ph/0611234] [INSPIRE].

[66] A. Kulesza and W.J. Stirling, *Nonperturbative effects and the resummed Higgs transverse momentum distribution at the LHC*, *JHEP* **12** (2003) 056 [hep-ph/0307208] [INSPIRE].

[67] A. Banfi, G.P. Salam and G. Zanderighi, *NLL+NNLO predictions for jet-veto efficiencies in Higgs-boson and Drell-Yan production*, arXiv:1203.5773 [INSPIRE].

JHEP06(2012)132